ABCM 40 anos
Associação Brasileira de Engenharia e Ciências Mecânicas

CONEM 2016
CONGRESSO NACIONAL DE ENGENHARIA MECÂNICA

21 - 25
AGOSTO DE 2016
FORTALEZA - CEARÁ

SCRAMJET DESIGN FOR INVESTIGATION ON SUPERSONIC COMBUSTION WITH LASER ENERGY ADDITION

Felipe Jean da Costa, felipejean@ieav.cta.br[1]
Tiago Cavalcanti Rolim, tiagorolim@ieav.cta.br[2]
Ronaldo de Lima Cardoso, ronaldolcardoso@yahoo.com.br[1]
Gustavo Jean da Costa, gustavojean15@hotmail.com[3]
Israel da Silveira Rêgo, israel.rego@ieav.cta.br[2]
Marco Antônio Sala Minucci, marco.salaminucci@gmail.com[2]
Antonio Carlos de Oliveira, acoc@ieav.cta.br[2]
Paulo Gilberto de Paula Toro, toro@ieav.cta.br[2]

[1]ITA - Instituto Tecnológico de Aeronáutica, Praça Marechal Eduardo Gomes, nº 50 Vila das Acácias CEP. 12.228-900 São José dos Campos, SP - Brasil
[2]IEAv - Instituto de Estudos Avançados, Trevo Coronel Aviador José Alberto Albano do Amarante, nº 1 Putim CEP. 12.228-001 São José dos Campos, SP - Brasil
[3]Fatec - Faculdade de Tecnologia de São José dos Campos - Prof. Jessen Vidal, Av. Cesare Mansueto Giulio Lattes, nº 1350 Eugênio de Melo CEP. 12.247-014 São José dos Campos, SP - Brasil

Abstract: *Laser energy addition in supersonic combustion has been investigated, in the Prof. Henry T. Nagamatsu Laboratory of Aerothermodynamics and Hypersonics, in order to reduce the drag, to promote supersonic air mixing with fuel, to improve combustion efficiency and to reduce the ignition time (and consequently combustor length), and acting as a flame holder. This paper presents a methodology to design a scramjet model (inlet-combustor) for laser energy addition in supersonic combustion for experimental investigation at the Hypersonic Shock Tunnel T3. In the aerodynamic design of scramjet with one compression ramp, flying at 30 km altitude with Mach number 7, one may considered the following steps: i) air flow with perfect gas behavior, inviscid (no boundary layer), and mass flow captured by the scramjet inlet will pass through the scramjet engine combustor (so that the incident shock wave of the compression system focuses in the cowl leading edge (shock-on-lip) and the reflected shock wave focuses at the combustion chamber entry (shock-on-corner), ii) boundary layer (viscous effects); and iii) fuel injection. It should be noted that the methodologies addressed obey the fundamental principles of physics with respect to the Mass, Linear Momentum and Energy. The quantification of the fundamental principles of physics is carried out through the Navier-Stokes Equations, which are valid, a priori, to continuous medium (altitudes up to 100 km). In general, Navier-Stokes Equations may applied for transient flow; incompressible or compressible; laminar and turbulent; neglecting field forces, volumetric heating and mass diffusion. Finally, oblique shock wave theory and one-dimensional flow with friction theory, which are based on the Navier-Stokes Equations, may be applied at the inlet and combustor sections of the scramjet experimental model. Fuel injection will be considered in order to determine the mix, ignition and reaction times, and consequently the total combustor length.*

keywords: *scramjet, Hypersonics, Laser Energy Addition, Supersonic Combustion.*

1. INTRODUCTION

The interest in laser energy addition in supersonic combustion has increased along the past years, in the sense to reduce the drag, supersonic air mixing with fuel, combustion efficiency improvements and reduction of the ignition time (Fendell et al., 1993; Horisawa et al., 2004; Tsuchiya et al., 2003), and as a flame holder (Brieschenk; et al., 2013). This paper presents a methodology to design a scramjet engine (Fig.1), inlet-combustor, for laser energy addition in supersonic combustion studies, considering the flight conditions at 30 km altitude and the conditions at the Hypersonic Shock Tunnel T3 of the Prof. Henry T. Nagamatsu Laboratory of Aerothermodynamics and Hypersonics.

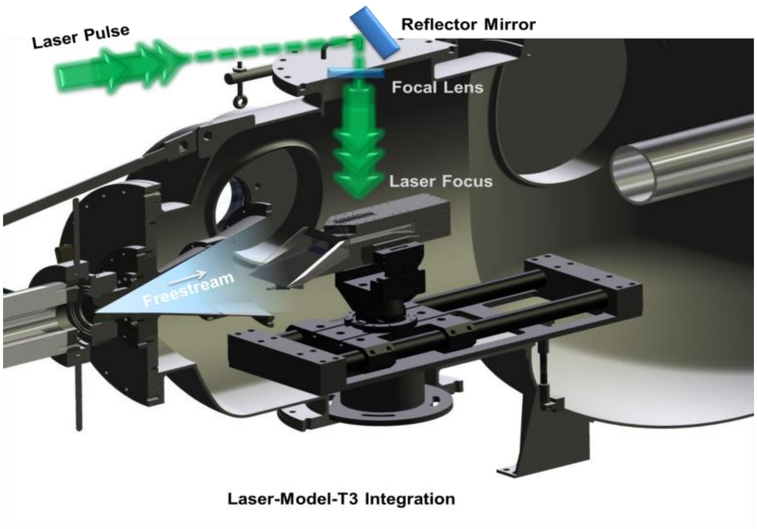

Figure 1. Experimental apparatus for investigation on supersonic combustion with laser energy addition.

2. AERODYNAMIC DESIGN

The aerodynamic design of the scramjet engine with one compression ramp considers: i) air in perfect gas behavior, inviscid flow (no boundary-layer), shock-on-lip and shock-on-corner conditions where the mass flow captured by the scramjet inlet will pass through the scramjet engine combustor (so that the incident shock wave of the compression system focuses in the cowl leading edge (shock-on-lip) and the reflected shock wave focuses at the combustion chamber entry (shock-on-corner), ii) viscous effects (boundary-layer) considering the displacement thickness approach, and iii) fuel injection evaluating the wall injection angles in order to determine the combustor length (based on the necessary time to fuel/air reaches the complete mixture, ignition time and reaction time), considering the constant area approach.

It was studied a compression ramp with 19 degrees, in the sense to reach a satisfactory result limited by the temperature (above 850 *K*) for the hydrogen self-ignition, pressure around 1 *atm*, and supersonic speed correspondent to Mach number 2.6, at the combustor entry. Once set the basic geometry of the inlet, the leading edge of the scramjet cowl must be replaced due the boundary-layer existence. The presence of the boundary-layer at the compression ramp will cause an estrangement of the shockwave angle from the compression ramp that originated it. In this case, we need to consider that the boundary-layer will originate a virtual compression ramp, and this phenomenon is called displacement thickness of the compression ramp. At the combustor, the influence of the boundary-layer will change the height of the combustor.

2.1. Oblique Shock Relations

The oblique shockwave with β angle is caused when the incident flow meets a positive deflection with θ angle (compression ramp). The deflection of the flow increases the aerothermodynamic properties (pressure, temperature, density and speed of sound), and decreases the speed and Mach number. Considering the flow speed may be decomposed in the perpendicular and tangential speeds to the oblique shockwave u_n and u_t, respectively, and the flow is inviscid, adiabatic, steady state without field forces and that there is no mass diffusion. The Eqs. 1-6, show the oblique shockwave relations, considering the air as calorically perfect gas:

$$M_{n1} = M_1 \sin \beta \tag{1}$$

$$\frac{p_2}{p_1} = 1 + \frac{2\gamma}{\gamma+1}\left(M_{n1}^2 - 1\right) \tag{2}$$

$$\frac{\rho_2}{\rho_1} = \frac{u_{n1}}{u_{n2}} = \frac{M_1^2(\gamma+1)}{2+(\gamma-1)M_1^2} \tag{3}$$

$$\frac{T_2}{T_1} = \frac{h_2}{h_1} = \frac{p_2}{p_1} \Big/ \frac{\rho_2}{\rho_1} \tag{4}$$

$$M_{n2}^{2} = \frac{1 + \frac{\gamma - 1}{2} M_{n1}^{2}}{\gamma M_{n1}^{2} \frac{\gamma - 1}{2}} \tag{5}$$

$$M_{2} = \frac{M_{n2}}{\sin\left(\beta - \theta\right)} \tag{6}$$

Using some numerical method (Newton-Raphson, secant, etc.) we can obtain the β shockwave, in relation to local flow deflection θ, throughout the equation:

$$\tan\theta = 2\cot\beta\left[\frac{M_{1}^{2}\sin^{2}\beta - 1}{M_{1}^{2}\left(\gamma + con2\beta\right) + 2}\right] \tag{7}$$

2.2. Boundary-Layer

The viscous effects have an important influence on the flow, because will introduce a new deflection angle θ at the compression ramp and will change the aerothermodynamic property values, consequently. For this purpose, this work considers the (laminar) displacement thickness δ^{*} approach, which represents the physical distance where the inviscid flow is displaced from its initial place due the boundary-layer presence, originating a virtual ramp (Fig. 2).

We can define the displacement thickness δ^{*} through Chapman-Rubesin theory, as follow (Bonelli, 2011):

$$\frac{\delta^{*}}{s_{3}} = \sqrt{\frac{C^{*}}{\mathrm{Re}_{s_3}}}\left[1{,}72 + 2{,}21\left(\frac{\gamma - 1}{2}\right)M_{2}^{2} + 1{,}93\left(\frac{T_{w} - T_{aw}}{T_{2}}\right)\right] \tag{8}$$

where, s_3 corresponds to the tangential coordinate to the wall (Eq. 9), C^{*} is the Chapman-Rubesin constant, Re is the Reynolds number, γ is the ratio of the specific heats, M is the Mach number, and the subscripts w and aw represent, respectively, the wall and adiabatic wall conditions. The local Reynolds number based on the s_3 coordinate (Fig. 2) is given by Eq. 10:

$$s_{3} = \frac{X_{3}}{\cos\theta} \tag{9}$$

$$\mathrm{Re}_{s_3} = \frac{\rho_{2} V_{2} s_{3}}{\mu_{2}} \tag{10}$$

where, the subscript *2* corresponds to the upstream oblique shockwave conditions.

The Chapman-Rubesin constant could be expressed by:

$$C^{*} = \frac{T_{2}\mu^{*}}{T^{*}\mu_{2}} \tag{11}$$

where, the superscript * corresponds to the properties evaluated to the reference enthalpy.

The dynamic viscosity was obtained by Sutherland's law:

$$\mu = 1{,}7894x10^{-5}\left(\frac{T}{288{,}16}\right)^{3/2}\frac{398{,}16}{T + 110} \tag{12}$$

The reference temperature is calculated by:

$$\frac{T^*}{T_1} = 0{,}28\frac{Te}{T_1} + 0{,}5\frac{Tw}{T_1} + 0{,}22\frac{Taw}{T_1} \tag{13}$$

Assuming:

$$\frac{Te}{T_2} = 1 \tag{14}$$

where, the subscript *e* corresponds to the properties at the edge of the boundary-layer.

The adiabatic wall temperature, which represents the maximum temperature inside the boundary-layer, may be obtained by:

$$\frac{Taw}{T_2} = 1 + r\frac{\gamma - 1}{2}M_2^2 \tag{13}$$

where, r is the recovery factor given by $r = \sqrt{\Pr}$ for laminar flow and $r = \sqrt[3]{\Pr}$ for turbulent flow (Schlichting, 1979), in this case *Pr* represents the Prandtl number assumed as 0,71, for this being value be a good approximation up to temperatures near 800 K (Anderson, 2010). In the absence of the temperature profile at the wall was chosen to assume the adiabatic condition on the wall $Tw = Taw$.

To obtain the effective geometry of the inlet considering the displacement thickness, we need to follow six steps, as described:

1. Evaluate the thermodynamics properties considering inviscid flow;
2. Calculate the displacement thickness δ^* through Chapman-Rubesin theory;
3. Based on the displacement thickness δ^* get a new compression ramp with the effective angle θ_{eff} ;
4. The thermodynamics properties values one may be recalculated, based on θ_{eff} ;
5. The process 2-4 one may be iterated up to reach the convergence for the θ_{eff} ;
6. Finally, the geometry must be adjusted due the boundary-layer presence.

The displacement thickness will be necessary to adjust the inlet geometry (Fig. 2) in order to satisfy the continuity, and to cancel the reflected oblique shockwave at the combustor entry.

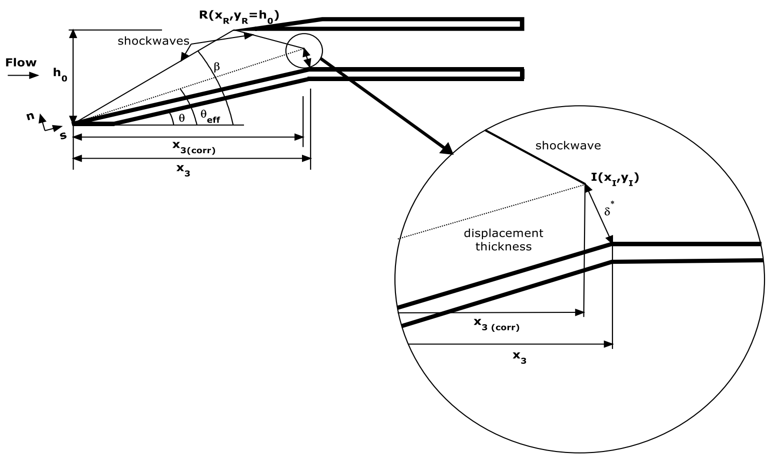

Figure 2. Boundary layer considering displacement thickness.

On the Fig. 2 h_0 represents the height of the inlet air capture between the compression ramp leading edge and the cowl leading edge, x_3 is the horizontal coordinate between compression ramp leading edge and the combustor entry. The dimension $x_3(corr)$ indicates the corrected horizontal coordinate for the new start point of the combustor entry. The points *R* and *I* are the reflection vertex of the oblique shockwave at the cowl leading edge and intersection between the reflected oblique shockwave and the boundary-layer, respectively.

θ_{eff} could be obtained by Eq. 14, using a iterative method:

$$\tan\theta_{eff} = \frac{x_3 \tan\theta + \delta^* / \cos\theta_{eff}}{x_3} \tag{14}$$

The coordinates of intersection point between the boundary-layer and oblique shockwave (Fig. 2) are described:

$$x_1 = \frac{y_R + \tan\alpha + x_R}{\tan\theta_{eff} + \tan\alpha} \tag{15}$$

$$y_1 = \tan\theta_{eff}\, x_1 \tag{16}$$

where, x_R and y_R (Eqs. 17-18) correspond to the vertex coordinates of the scramjet cowl, where will occur the reflection of oblique shockwave. The α angle is the reflected shockwave angle, calculated by Eq. 19:

$$y_R = h_0 \tag{17}$$

$$x_R = \frac{b_0}{\tan\beta_R} \tag{18}$$

$$\alpha = \beta_R - \theta_{eff} \tag{19}$$

3. COMBUSTOR DESIGN

3.1. Combustor dimensioning

Following the terminology applied to sections of a scramjet defined by Heiser and Pratt (1994), Fig. 3, we have the compression sections (internal and external), the combustor and expansion (internal and external) which allow the analysis of thermodynamic cycle and consequent design of the scramjet engine components (Costa, 2011).

The inlet produces suitable conditions of pressure and temperature to occur in the ignition fuel-air mixture. The region between points 0 and 1 corresponds to the inlet external compression section. Between points 1 and 3, there is the inlet internal compression section. Among the points 3 and 4 the fuel is injected into the combustion chamber section, where it will be mixed with atmospheric air at supersonic speed. The pre-expansion occurs between points 4 and 9, the effect to prevent the thermal choke due the heat addition with constant area combustor. The region between the points 9 and 10 is responsible for external expansion of the combustion products.

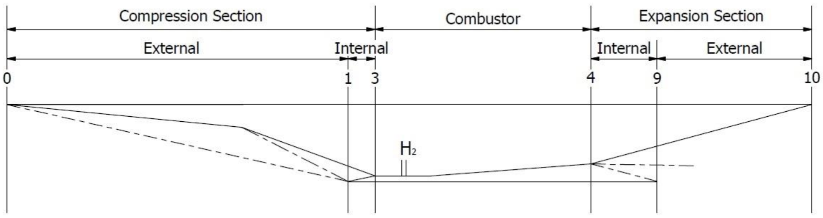

Figure 3. Terminology applied to the scramjet sections (Costa, 2011).

The height of the combustor could be given by continuity equation:

$$\dot{m} = \rho_0 u_0 A_0 = \rho_1 u_1 A_1 = \rho_2 u_2 A_2 = \rho_3 u_3 A_3 \tag{20}$$

where, $\dot{m}$ is the mass flow and *A* corresponds to the cross-section.

For a combustor with rectangular geometry, we have that the height of combustor *h* could be obtained by:

$$h = \frac{\dot{m}}{\rho_3 u_3 L} \tag{21}$$

where, L is the combustor width.

The position of the cowl leading edge corresponds to the horizontal line of the point of intersection that limit the capture area A_0, design point, and the oblique shockwave originated at the edge compression ramp (Fig. 4), establishing the *shock-on-lip* (*SOL*) condition to minimize the flow spillage. The position of compression ramp end is determined by its intersection with the reflected oblique shockwave coming from the cowl leading edge (Fig. 4).

h_0 is the height between the vehicle leading edge and the cowl leading edge (given by the point of incidence $R(x_R, y_R)$), defining the air capture (Fig. 4). θ and β correspond to deflection and oblique shockwave angles. The reflected oblique shockwave angle is given by $\beta_R - \theta$. The height of the combustion chamber is given by h_3 and considering constant area, $h_3 = h_4$. The coordinates x_3, x_{inj} and x_4 correspond to the length of the compression ramp, horizontal location of the injectors (defined as design premise the value of 20 mm from x_3) and total length of the scramjet engine, respectively. It is noteworthy that in this project was neglected the isolator section, and the beginning of the combustor is immediately after the compression ramp.

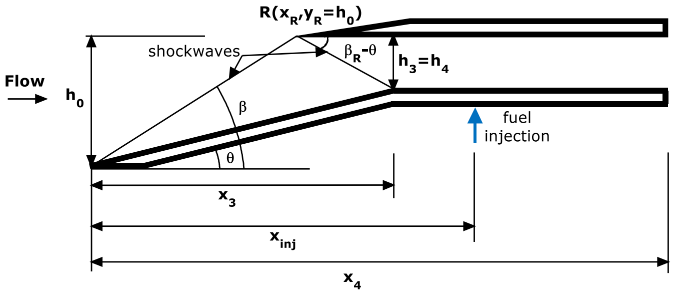

Figure 4. Shock-on-lip condition with the shockwaves focusing at the cowl leading edge vertex and combustor entry.

3.2. Fuel injection

For the fuel injection model, we use the concept of mixing efficiency. The mixing efficiency is defined as the ratio between the amount of fuel available for the reaction and the total amount of fuel injected. Based on experimental data, the mixing efficiency for axial injection is a function of the axial distance and the required distance for complete mixing of the reactants (Northam; Anderson, 1986). The mixing efficiency for axial may then is given as:

$$\eta_{0^\circ} = x/L_M \tag{22}$$

$$\frac{L_M}{b} = \begin{cases} 0.179 C_M e^{1.72\phi_0}, \phi_0 \le 1.0 \\ 3.333 C_M e^{-1.204\phi_0}, \phi_0 > 1.0 \end{cases} \tag{23}$$

given that b is the height of the combustor duct and C_M is an empirical constant of mixing rate ranging from 25 to 60 (Pulsonetti; Erdos; Early, 1991). In this work, it was considered $C_M = 25$ ($C_M = 60$ in the model of Northam and Anderson (1986)). In the case of normal fuel injection, we have:

$$\eta_{90^\circ} = 1.01 + 0.176 \ln\left(\frac{x}{L_M}\right) \tag{24}$$

This mixture model, once known values of the mixing efficiency for axial and normal cases, we can obtain the values for injection angles between 0°-90°, applying a linear interpolation.

3.3. Ignition and reaction times

There are four parameters that must be known for the occurrence of self-ignition and subsequent combustion, they are static temperature, static pressure, fuel-air mixture, and residence time. Thus, we can define the ignition time t_i as the necessary time, from ignition until 95% of the heat is released, via the formation of products, in this case H_2O.

$$t_i = \frac{L_i}{u_3} = \frac{8x10^{-9} e^{\frac{9600}{T}}}{p} \tag{25}$$

in this relation, *p* is in *atm* and *T* in *K*.

Equation 28 is relative to the reaction time t_r:

$$t_r = \frac{L_r}{u_3} = \frac{1.05x10^{-4} e^{\frac{-1.12T}{1000}}}{p^{1.7}} \tag{26}$$

The nonlinear variation og the ignition temperature for a mixture hydrogen-air is because the reagent has power able to overcome the activation energy needed to start the chain reaction. The likelihood of an ignition may be small if the reagents energy levels are close to the minimum value, and thus the ignition time will be much higher. Whereas the hydrogen self-ignition temperature is close to 800 *K*, and if we work close to this temperature at which the ignition time will tends to infinity, and consequently, there will be no self-ignition. There will be no great energy of activation after ignition due to the fact that there are already formed reactive chain carriers (Huber, *et al.*, 1979).

4. RESULTS

This engine was designed to meet a mission considering the speed correspondent to Mach number 7 and 30 *km* altitude. Furthermore, the test platform will be mounted on T3 Hypersonic Shock Tunnel. Table 1 shows the values of the thermodynamic properties and flow velocity considering project altitude (U.S. Standard Atmosphere, 1976).

Table 1.Thermodynamic Properties and Mach number.

Condition	Temperature [*K*]	Pressure [*Pa*]	Density [*kg/m³*]	Speed of Sound [*m/s*]	Mach Number
30 km	226.50	1197	$1.841x10^{-2}$	301.70	7.00

4.1. Inlet

The assumption is based on ensuring a temperature at the combustor entry between 1000-2000 *K* and a pressure of 0.25-1.00 *atm*, in order to have an effective combustion in a combustor with a reasonable length (O'Neill; Lewis, 1992). The lower limit of this temperature range and pressure is determined by the hydrogen-air reaction mechanism. However, the upper limit is linked to the fact that the excessive temperature rise would cause the dissociation of the air and consequently lower combustion efficiency. Furthermore, to have the upper limit of the condition would be necessary to increase the number of ramps for the compression system, which would result in a vehicle/model large. For inviscid flow case we defined the combustor height as 15 *mm*, and using the equations presented on section 2.1 we obtain the thermodynamic properties inside the combustor as show Table 2, at 30 *km* altitude. The Fig. 5 shows the preliminary inlet dimensions, considering the inviscid flow approach.

Table 2. Thermodynamic Properties of the inlet at 30 km altitude.

Properties	Final of External Compression (Station 1)	Final of Internal Compression (Station 3)	Units
M	3.8	2.53	-
T	628.6	1071	*K*
p	13052.77	59973.88	*Pa*
ρ	$7.23x10^{-2}$	$1.95x10^{-1}$	*kg/m³*
a	502.59	656.07	*m/s*
u	1911.09	1662.27	*m/s*
β	26.11	32.09	*degrees*

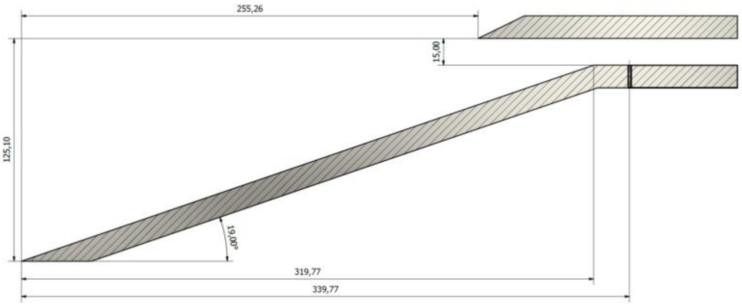

Figure 5. Inlet dimensions considering inviscid flow.

4.2. Boundary-layer influence

Table 3 shows the values of the thermodynamic properties calculated for the station 1 of the scramjet engine, besides the Mach number, the properties versus the reference temperature, the value of δ^*. To obtain the values shown in Table 3 were performed six iterations. Based on the properties found for the scramjet station 1 (Table 3) were calculated the thermodynamic properties, Mach number and angle of the reflected oblique shockwave at the station 3 of scramjet engine and is shown in Table 4. Also, Table 4 shows θ_{eff} , β and $\alpha = \beta_R - \theta_{eff}$ angles that correspond to the effective angle of the compression ramp, oblique shockwave and reflected oblique shockwave angle, considering viscosity. The coordinates x_R, y_R, x_i and y_i corresponding to *R* and *I* points (vertices of reflection of the oblique shockwave at the cowl leading edge and the intersection of reflected oblique shockwave and boundary layer, respectively) were calculated from the new compression ramp angle called θ_{eff} (Table 4) and are presented in Table 5.

Table 3. Thermodynamic Properties and Mach number to calculate the displacement thickness δ^*, after six iterations.

Properties	Value	Units
M_1	3.83	-
ρ_1	7.19x10^{-2}	*kg/m³*
T_1	621.2	*K*
a_1	301.7	*m/s*
μ_1	3.09x10^{-5}	*Kg/(m.s)*
$Tw = Taw$	2249.3	*K*
T^*	1793.4	*K*
μ^*	5.81x10^{-5}	*Kg/(m.s)*
C^*	6.53x10^{-1}	-
$\mathrm{Re}_{1,x}$	1.47x10^{6}	-
δ^*	1.80x10^{-3}	*m*

Table 4. Thermodynamic Properties and Mach number to calculate the displacement thickness δ^*, after six iterations.

Properties	Value	Units
M_3	2.55	-
ρ_3	1.95x10^{-1}	*kg/m³*
T_3	1063.1	*K*
p_3	59461.55	*Pa*
u_3	31.97	*degrees*

β_R	1666.60	*m/s*
θ	19	*degrees*
θ_{eff}	19.31	*degrees*
β	25.86	*degrees*
$\beta_R - \theta_{eff}$	12.66	*degrees*

Table 5. Thermodynamic Properties, Mach number after reflected oblique shockwave and coordinates of intersection and reflection points, considering δ^*.

Properties	Value	Units
x_R	0.2581	*m*
$y_R = h_0$	0.1251	*m*
$x_1 = x_3$	0.323	*m*
y_1	0.1099	*m*
h_4	0.01678	*m*
x_{inj}	0.343	*m*

4.3. Combustor length

Table 6 shows the required length for complete fuel-air mixture to the case of axial fuel injection $(L_{m,axial})$ and fuel injection normal to the direction of flow inside the combustor $(L_{m,normal})$. Also, are presented in Table 7 the $x_{ign}, x_{rea}, x_{4axial}$ and $x_{4normal}$ lengths, required for the occurrence of ignition and reaction, total length, considering axial and normal fuel injection, respectively. Finally, Table 6 shows the required times for ignition and reaction t_{ign} and t_{rea} respectively.

Table 6. Required lengths and necessary times to occur ignition and reaction.

Properties	Value	Units
$L_{m,axial}$	0.11545	*m*
$L_{m,normal}$	0.03135	*m*
x_{ign}	0.18974	*m*
x_{rea}	0.13165	*m*
x_{4axial}	0.77985	*m*
$x_{4normal}$	0.69575	*m*
t_{ign}	$1.139\text{x}10^{-4}$	*s*
t_{rea}	$7.90\text{x}10^{-5}$	*s*

The Fig. 6 corresponds to the effective geometry of the scramjet engine, as result of presented approaches at the adopted methodologies of this work.

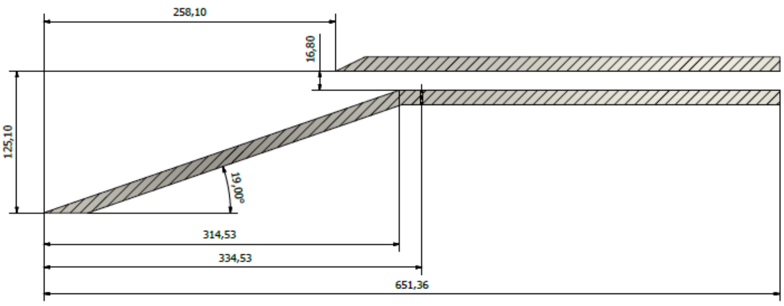

Figure 6. Inlet and combustor final dimensions.

5. CONCLUSION

In this study, we sought a scramjet configuration that meets, according to O'Neill and Lewis (1992), the necessary conditions for self-ignition of hydrogen, being between 1000-2000 *K* and pressure of 0.25-1, 00 *atm*, so as to ensure a combustion process efficiently in a compact length of the combustor. It is concluded that the design, presented in this paper covers the main methodologies for the development of a scramjet engine aiming the combustion efficiency and for the laser energy addition experimental research. Studies in order to develop a combustor with constant pressure considering energy addition, chemical equilibrium, and 10 chemical species for the combustion process have been developed.

6. ACKNOWLEDGMENTS

The last author would like to express gratitude to FINEP (agreement nº 011015601), and the first author to thank the CNPq (process nº 376505/2014-1), for the financial support.

7. REFERENCES

Anderson, J. D. JR. Modern compressible flow. 3rd. ed. McGraw-Hill, 2003.

Bonelli, F. Preliminary Design of a Hypersonic Air-breathing Vehicle. Flux, n. April, p. 1–14, 2011.

Brieschenk, Stefan; O’Byrne, Sean; Kleine, Harald. Laser-induced plasma ignition studies in a model scramjet engine. Combustion and Flame, v. 160, n. 1, p. 145–148, 2013.

Costa, Felipe Jean Da. Projeto dimensional para manufatura do veículo hipersônico aeroespacial 14-X. 2011. 79 f. FATEC Prof. Jessen Vidal, 2011.

Fendell, F et al. Laser-initiated conical detonation wave for supersonic combustion. II. Journal of Propulsion and Power, doi: 10.2514/3.23607, v. 9, n. 2, p. 182–190, 1 mar. 1993.

Heiser, Willian H.; Pratt, David T. Hypersonic Airbreathing Propulsion. Washington, D. C.: AIAA Education Series, 1994.

Horisawa, Hideyuki et al. Effects of a focused laser pulse for combustion augmentation characteristics in supersonic airstreams. Vacuum, v. 73, n. 3-4, p. 439–447, abr. 2004.

Huber, Paul W.; Schexnayder, Charles J.; MCclinton, Charles R. Criteria for self-ignition of supersonic hydrogen-air mixtures. NASA Technical Paper 1457. , 1979

Kremeyer, Kevin; Sebastian, Kurt A; Shu, Chi-Wang. Computational Study of Shock Mitigation and Drag Reduction by Pulsed Energy Lines. AIAA Journal, doi: 10.2514/1.17854, v. 44, n. 8, p. 1720–1731, 1 ago. 2006.

Northam, G; Anderson, G. Survey of supersonic combustion ramjet research at Langley. 24th Aerospace Sciences Meeting. Aerospace Sciences Meetings. American Institute of Aeronautics and Astronautics, 1986.

O’Neill, Mary Kae Lockwood; Lewis, Mark J. Optimized Scramjet Integration on a Waverider. Journal of Aircraft, v. 29, n. 6, p. 1114–1121, 1992.

Pulsonetti, Maria V.; Erdos, John; Early, Kevin. Engineering model for analysis of scramjet combustor performance with finite-rate chemistry. Journal of Propulsion and Power, v. 7, n. 6, p. 1055–1063, 1991.

Schlichting, H. Boundary-Layer Theory. New York: McGraw-Hill Series in Mechanical Engineering, 1979.

Tsuchiya, Shuhei et al. Ignition Characteristics of Laser-Induced Plasmas in Supersonic Combustion. 39th AIAA/ASME/SAE/ASEE Joint Propulsion Conference and Exhibit. Joint Propulsion Conferences. American Institute of Aeronautics and Astronautics, 2003.

U.S. Standard Atmosphere. NASA TM-X 74335. Washington, D. C.: National Oceanic and Atmospheric Administration, National Aeronautics and Space Administration and United States Air Force. , 1976

Van Wie, D. M. Scramjet Inlets. Scramjet Propulsion. Progress in Astronautics and Aeronautics. American Institute of Aeronautics and Astronautics, 2001. p. 447–511.

8. AUTHORIAL RESPONSIBILITY

“The authors are the unique responsible for the content of this work”.